Report

Neuron

Gradual Suppression of Transcytosis Governs Functional Blood-Retinal Barrier Formation

Highlights

- Retinal vessels at P1 have functional tight junctions but display bulk transcytosis
- Immature vessel leakage is entirely due to transcytosis and not via tight junctions
- Gradual suppression of transcytosis governs functional blood-retinal barrier formation
- Retinal vasculature is a tractable system to study CNS barriers

Authors

Brian Wai Chow, Chenghua Gu

Correspondence

chenghua_gu@hms.harvard.edu

In Brief

Chow and Gu characterized the spatio-temporal development of functional blood-retinal barrier formation and demonstrated that immature vessel leakage is entirely due to bulk transcytosis and not via tight junctions. Gradual suppression of transcytosis determines functional blood-retinal barrier formation.

Chow & Gu, 2017, Neuron *93*, 1325–1333
March 22, 2017
http://dx.doi.org/10.1016/j.neuron.2017.02.043

CellPress

Neuron
Report

Gradual Suppression of Transcytosis Governs Functional Blood-Retinal Barrier Formation

Brian Wai Chow[1] and Chenghua Gu[1,2,*]
[1]Department of Neurobiology, Harvard Medical School, 220 Longwood Ave., Boston, MA 02115, USA
[2]Lead Contact
*Correspondence: chenghua_gu@hms.harvard.edu
http://dx.doi.org/10.1016/j.neuron.2017.02.043

SUMMARY

Blood-central nervous system (CNS) barriers partition neural tissues from the blood, providing a homeostatic environment for proper neural function. The endothelial cells that form blood-CNS barriers have specialized tight junctions and low rates of transcytosis to limit the flux of substances between blood and CNS. However, the relative contributions of these properties to CNS barrier permeability are unknown. Here, by studying functional blood-retinal barrier (BRB) formation in mice, we found that immature vessel leakage occurs entirely through transcytosis, as specialized tight junctions are functional as early as vessel entry into the CNS. A functional barrier forms only when transcytosis is gradually suppressed during development. Mutant mice with elevated or reduced levels of transcytosis have delayed or precocious sealing of the BRB, respectively. Therefore, the temporal regulation of transcytosis governs the development of a functional BRB, and suppression of transcytosis is a principal contributor for functional barrier formation.

INTRODUCTION

Central nervous system (CNS) endothelial cells lining blood vessels form the blood-CNS barriers, which include the blood-brain barrier, blood-spinal cord barrier, and inner blood-retinal barrier (BRB) (Engelhardt and Coisne, 2011). These cells have two properties that limit the passage of substances between the blood and the CNS parenchyma: (1) specialized tight junction complexes between CNS endothelial cells prevent paracellular flux and (2) low rates of vesicular trafficking between the luminal and abluminal membrane, known as transcytosis, limit transcellular passage (Andreone et al., 2015; Chow and Gu, 2015; Raviola, 1977; Reese and Karnovsky, 1967; Zhao et al., 2015). Although tight junctions are thought to be the principal mechanism for establishing blood-CNS barriers, recent findings suggest that altered rates of transcytosis also influence barrier permeability (Ben-Zvi et al., 2014; Knowland et al., 2014). Barrier properties are not intrinsic to CNS endothelial cells but rather are acquired from the neural environment during development (Blanchette and Daneman, 2015; Hagan and Ben-Zvi, 2015; Stewart and Wiley, 1981). However, it is not understood when and how specialized tight junctions and suppression of transcytosis occur and what their relative contributions are in establishing a functional CNS barrier during development. Loss of barrier function is a hallmark of some CNS degenerative diseases (Obermeier et al., 2013; Winkler et al., 2014; Zlokovic, 2008). Yet, a functional barrier is also a major obstacle for CNS drug delivery (Banks, 2016). Dissecting the relative roles of tight junctions and transcytosis in regulating barrier permeability and elucidating the basic principles governing the establishment of CNS barrier properties will enable targeted manipulations of the barrier during disease.

The retinal vasculature is well suited to address many fundamental questions about CNS barriers. Physiologically analogous to the blood-brain barrier, the BRB regulates the optimal milieu for phototransduction. Unlike the complex brain vascular network, the retinal vasculature has a relatively simple, stereotypic development and architecture, consisting of a three-tiered, two-dimensional plexus (Stone et al., 1995). Mouse retinal angiogenesis occurs shortly after birth. CNS endothelial cells invade the optic nerve head and expand radially along the vitreal surface from the center toward the periphery, forming the entire primary plexus by postnatal day 8 (P8) (Figures 1A and 1B) (Fruttiger, 2007). Sprouts from the primary plexus then penetrate into the retina, forming the deeper plexus, followed by further sprouting to form the intermediate plexus (Stahl et al., 2010). Here, we use the BRB as a model system to elucidate the relative contributions of tight junctions and transcytosis in regulating CNS barrier permeability during development. To our surprise, we found that functional tight junctions are already present when vessels first entered the CNS so the gradual suppression of transcytosis in CNS endothelial cells governs the development of a functional barrier.

RESULTS

Functional BRB Is Formed Gradually and Is Fully Acquired by P10

We first mapped the spatio-temporal formation of the functional BRB. To evaluate BRB permeability, we transcardially injected mice at several postnatal ages with Sulfo-NHS-Biotin (550 Da) or fluorescently labeled, 10-kDa dextran tracer. A functional BRB, as in adults, completely confines both tracers within the vasculature (Figure S1A). However, at P1, when blood vessels

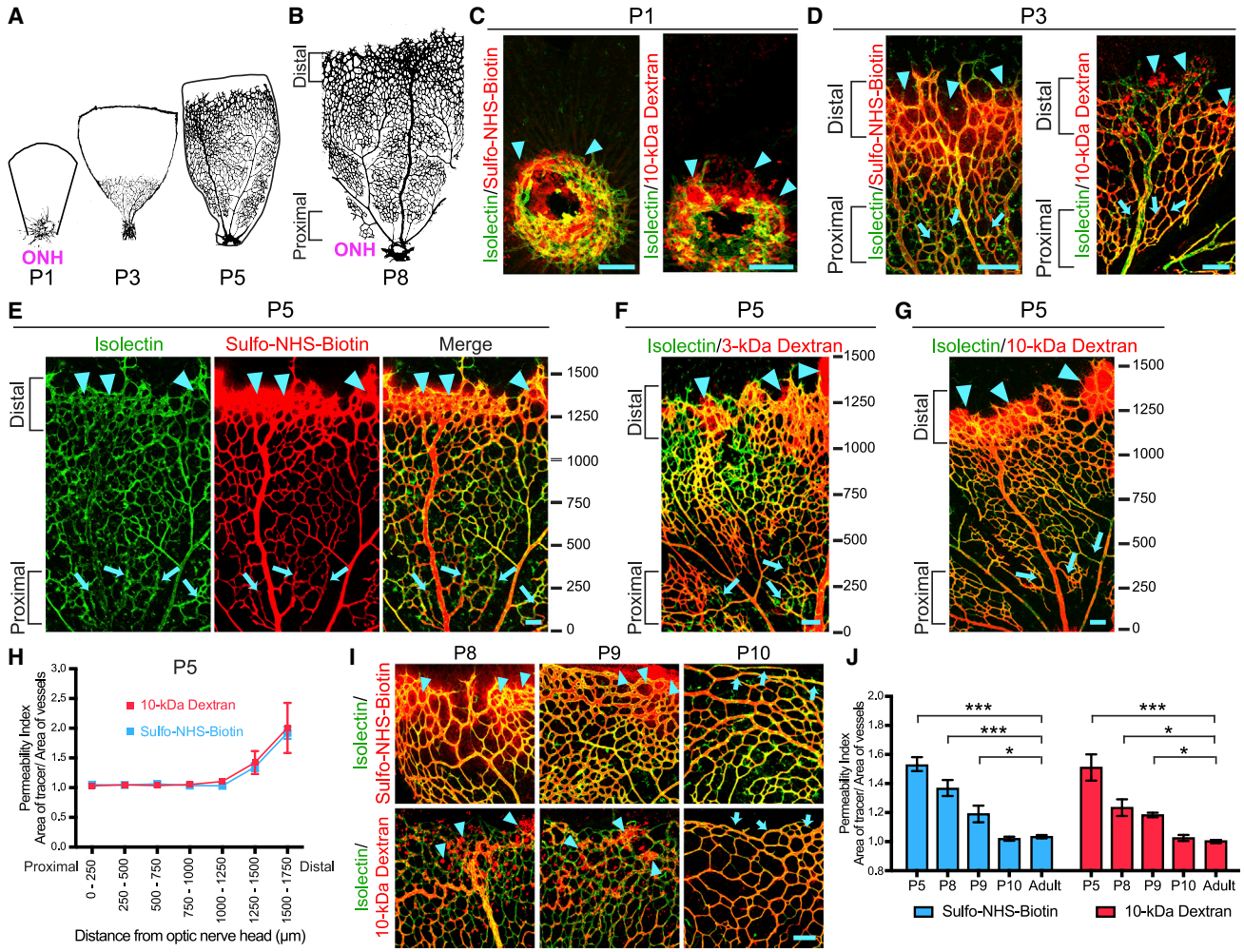

Figure 1. Spatio-Temporal Characterization of Functional BRB Formation

Intravenous injections of tracers in neonatal mice reveal that functional BRB is formed gradually from proximal to distal in the primary plexus.

(A and B) Spatio-temporal development of the mouse retina primary plexus. Vessel ingression at the optic nerve head (ONH) occurs at P1. Vessels then expand from the ONH to the retinal periphery during postnatal development (A). Vessels reach the peripheral edge of the retina at P8. A spatio-temporal gradient of vessel maturation is observed: the vessels proximal to the ONH are more mature, whereas the vessels distal to the ONH are nascent (B).

(C) In P1 retinas, when blood vessels (isolectin, green) first enter the retina, Sulfo-NHS-Biotin (left) and 10-kDa dextran (right) tracer (red) leakage is observed around budding vessels (arrowheads).

(D–G) In P3 (D) and P5 (E–G) retinas, a gradient of barrier functionality is observed. More mature vessels proximal to the ONH confine tracer (arrows), whereas nascent vessels distal to the ONH leak tracer (arrowheads). Ticks in (E)–(G) represent distance in microns from the ONH. 0 is slightly before the ONH.

(H) Permeability index of P5 retinas from tracer-injected pups reveals the functional BRB is gradually formed in a proximal-to-distal fashion. The permeability index is measured by the ratio of tracer-positive area over isolectin-positive area. A ratio greater than 1 indicates that the BRB is permeable and immature. A ratio of 1 indicates that the BRB is impermeable and hence mature. 250 μm^2 fields of view were sampled and tiled starting from 0 to the angiogenic front. The average distance from the ONH to the angiogenic front at P5 is 1,651 ± 288 μm. Data are mean ± SEM (n = 5–6).

(I) Higher magnification of distal vessels of the primary plexus show Sulfo-NHS-Biotin (top) and 10-kDa dextran (bottom) tracer leakage at P8 and P9 (arrowheads). At P10, both tracers are confined in distal vessels (arrows).

(J) Quantification of distal vessel permeability for Sulfo-NHS-Biotin and 10-kDa dextran throughout BRB development. Data are mean ± SEM (n = 5–6 mice per age per tracer group from three different litters). Statistical significance was determined by one-way ANOVA with a post hoc Bonferroni multiple comparison adjustment, comparing the various neonatal ages with the adult in the respective Sulfo-NHS-Biotin and 10-kDa dextran group. *$p < 0.05$, ***$p < 0.001$. Scale bar represents 100 μm for all panels.

See also Figures S1, S2, and S5.

first enter the retina through the optic nerve head and are ensheathed by pericytes (Figure S2A), leakage of both tracers into the retinal parenchyma from the budding vessels was evident (Figure 1C), indicating that these developing vessels do not intrinsically have a functional barrier. In P3 and P5 retinas, both tracers leaked into the parenchyma and were taken up by non-vascular cells near nascent vessels at the angiogenic front, located distal to the optic nerve head (Figures 1D–1G,

arrowheads), while both tracers were confined in the more mature vessels located proximal to the optic nerve head (Figures 1D–1G, arrows). Indeed, Sulfo-NHS-Biotin, 3-kDa dextran tracers, and 10-kDa dextran tracers at P5 reveal that a functional barrier is formed gradually in a proximal-to-distal fashion (Figures 1E–1H). At P8 and P9, although the angiogenic front reaches the retinal periphery, the nascent, distal vessels still exhibited leakage (Figures 1I and 1J), whereas the mature, proximal vessels confined Sulfo-NHS-Biotin and 10-kDa dextran tracers (Figures S1B and S1C). At P10, both tracers were completely confined in all vessels of the primary plexus, including distal vessels (Figures 1I and 1J; Figures S1B and S1C). Thus, these data demonstrate that developing vessels are initially leaky, that a functional barrier is formed gradually from proximal to distal, and that the primary plexus acquires a functional BRB by P10.

We next examined when the functional BRB is established in the deeper plexus, which sprouts from the primary plexus between P7 and P12. Sprouting vessels of the deeper plexus showed leakage of both Sulfo-NHS-Biotin and 10-kDa dextran tracers at P8 and P9 (Figures S1D and S1E). However, at P10, when the deeper plexus vessels continue to sprout, both tracers were confined in newly formed vessels (Figures S1D and S1E). Finally, we investigated when the BRB becomes functional in the intermediate plexus, which sprouts from the deeper plexus between P12 and P17. At P12, sprouting nascent vessels, surprisingly, already confined both tracers; no leakage was observed at any ages examined (Figures S1F and S1G). Together, these data demonstrate that the developing retinal vasculature does not intrinsically have a functional barrier but instead gradually acquires barrier properties. Once barrier properties are attained by P10, nascent vessels sprouting from vessels with a functional BRB inherit and maintain these barrier properties. Thus, the three-tiered retinal vasculature acquires a functional BRB remarkably by one distinctive age: P10 (Figure 1; Figure S1).

At P1, Budding CNS Endothelial Cells Possess Functional Tight Junctions but Display Bulk Transcytosis

We next addressed the subcellular mechanisms underlying functional BRB development. We asked whether CNS endothelial cells form functional tight junctions and acquire low rates of transcytosis synchronously or sequentially to establish the functional BRB and what the relative contribution of each property is to the regulation of BRB permeability. To evaluate the functionality of tight junctions and suppression of transcytosis at subcellular resolution, we injected horseradish peroxidase (HRP) intravenously at several ages and imaged the retina with transmission electron microscopy (EM). In the lung and heart vasculature, where barrier properties are absent, luminal HRP leaks into the basement membrane and parenchyma both by passing through junctions, observed as HRP-filled tight junctions, and by high rates of transcytosis, evident as numerous HRP-filled intracellular vesicles (Karnovsky, 1967; Schneeberger-Keeley and Karnovsky, 1968). However, in adult retinal endothelial cells, where barrier properties are present (Raviola, 1977; Reese and Karnovsky, 1967), we observed that luminal HRP is halted sharply at electron-dense "kissing points" between endothelial cells where adjacent membranes are tightly apposed (Figure 2A). Adult retinal endothelial cells also displayed few HRP-filled vesicles, indicating that transcytosis is suppressed (Figure 2B).

At P1, we observed tracer extravasation from budding vessels, indicating leaky vessels (Figure 1C). Surprisingly, under EM, these CNS endothelial cells already had specialized tight junctions that halted the HRP at the kissing points (Figures 2C and 2E), as observed in adult, mature CNS endothelial cells (Figure 2A). However, these CNS endothelial cells had many HRP-containing vesicles, including luminal and abluminal membrane-associated vesicles and cytoplasmic vesicles (Figures 2D and 2F), similar to lung and heart endothelial cells, where suppression of transcytosis is absent (Schneeberger-Keeley and Karnovsky, 1968). These results indicate that as early as vessel ingression at P1, functional tight junctions are present in budding CNS endothelial cells, but transcytosis has not been suppressed, suggesting that immature BRB leakiness is entirely due to uninhibited transcytosis.

Gradual Suppression of Transcytosis Governs Functional BRB Formation

To test the hypothesis that suppression of transcytosis determines functional BRB development, we used EM to examine vesicular trafficking at later postnatal ages. At P5 and P8, in distal, leaky vessels, many HRP-filled vesicles were observed (Figures 2G and 2H), indicating that transcytosis has not been suppressed. However, in the proximal vessels that are impermeable to tracer, very few HRP-filled vesicles were observed, suggesting that suppression of transcytosis had occurred (Figures S3A and S3C). By P10, when all the retinal vessels have a functional BRB, negligible HRP-filled vesicles were observed in both distal and proximal vessels (Figures 2G and 2H; Figures S2A and S2C). Consistent with the observation at P1, functional tight junctions were present in all vessels, both proximal and distal, at all ages tested (Figures 2I and 2J; Figures S3B and S3D). These data demonstrate that a leaky, immature barrier is due entirely to high rates of bulk transcytosis in endothelial cells. A functional barrier is established days later, only after transcytosis is suppressed, coinciding with functional BRB development by P10. Therefore, the spatio-temporal regulation of transcytosis governs the development of a functional BRB.

Mfsd2a Is Essential to Suppress Transcytosis at the Functional BRB

Given the significance of transcytosis in functional BRB formation, we next examined whether Mfsd2a, a known transcytosis regulator in blood-brain barrier formation (Ben-Zvi et al., 2014), also plays a role in BRB formation. EM analysis of retinas from HRP-injected adult mice revealed increased HRP-filled vesicle density in the CNS endothelial cells of *Mfsd2a*$^{-/-}$ mice compared to *Mfsd2a*$^{+/+}$ littermate controls (Figures 3A and 3B), whereas tight junctions remained functional (Figures 3C and 3D). Thus, Mfsd2a plays a similar role at the BRB in suppressing transcytosis.

Mfsd2a Expression Correlates with Functional BRB Formation

We next examined Mfsd2a expression as a marker for suppressed transcytosis during BRB development by immunostaining retinas

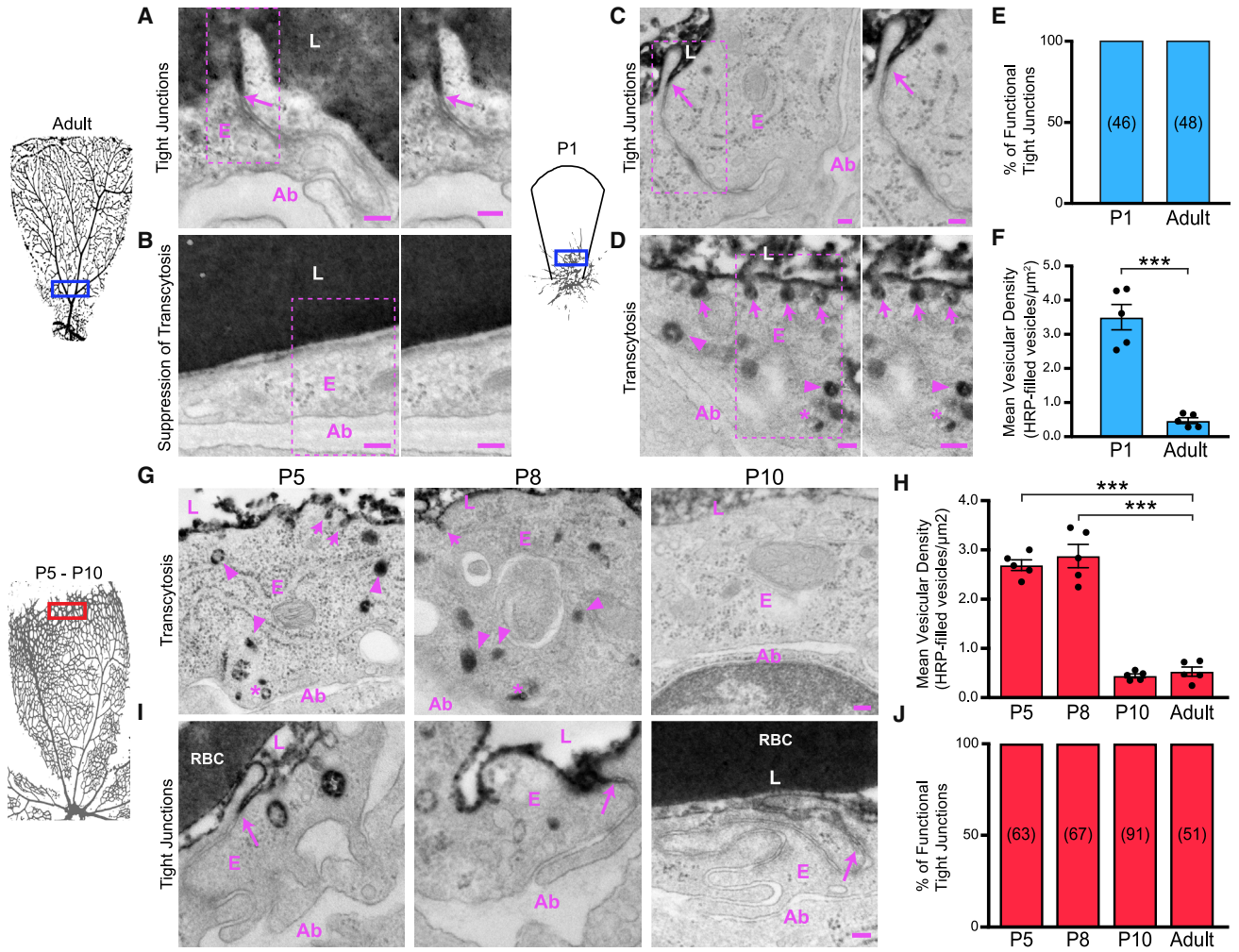

Figure 2. Gradual Suppression of Transcytosis Governs the Development of an Impermeable, Functional BRB

As early as P1, budding CNS endothelial cells possess functional tight junctions but display bulk transcytosis.

(A and B) EM of endothelial cells in the proximal retina of an HRP-injected adult mouse. Specialized tight junctions are functional and prevent electron dense 3-3′ diaminobenzidine (DAB) reaction product in the lumen from invading through the intercellular cleft (arrows) (A). Transcytosis was suppressed in endothelial cells as seen by negligible numbers of tracer-filled vesicles (B). Also shown is a magnification of the boxed areas.

(C and D) EM of endothelial cells in the proximal retina from an HRP-injected P1 pup. Tracer invades through the intracellular cleft between the endothelial cells but stops at junctions without invading to the abluminal side (arrows) (C). DAB reaction product filled the vesicles attached to the luminal membrane (arrows), in the cytoplasm (arrowheads), and near the abluminal membrane (asterisk) (D). Also shown is a magnification of the boxed areas.

(E) The percentage of functional tight junctions from the EM images (n = 5 mice per age; 15–20 vessels analyzed per mouse; number of tight junctions analyzed are displayed in parentheses).

(F) Number of tracer-filled vesicles in endothelial cells in P1 and adult mice. Data are presented as mean ± SEM (n = 5 mice per age; each circle represents the average vesicular density from 15–20 vessels per mouse). Statistical significance was assessed by unpaired t test. L, lumen; E, endothelial cell; Ab, abluminal. **p < 0.01. Scale bar represents 100 nm in all panels.

(G) At P5 and P8, many tracer-filled vesicles are observed at the luminal membrane (arrows), in the cytoplasm (arrowheads), and at the abluminal membrane (*) in distal endothelial cells. At P10, distal endothelial cells contain negligible numbers of tracer-filled vesicles.

(H) Number of tracer-filled vesicular densities in distal vessels at P5, P8, and P10. Data are shown as mean ± SEM (n = 5 mice per age; each circle represents the average vesicular density from 15–20 vessels per mouse). Statistical significance was determined by one-way ANOVA with a post hoc Bonferroni multiple comparison adjustment, comparing distal vessels of the various neonatal ages to distal vessels of adults.

(I) EM of distal vessels from P5, P8, and P10 retinas reveals tracer product halts at tight junctions (arrows) at all ages.

(J) Percentage of functional tight junctions from distal vessels (n = 5 mice per age; 15–20 vessels analyzed per mouse; number of tight junctions analyzed are displayed in the bars). L, lumen; E, endothelial cells; Ab, abluminal; RBC, red blood cell. ***p < 0.001. Scale bar represents 100 nm in all panels.

See also Figure S3.

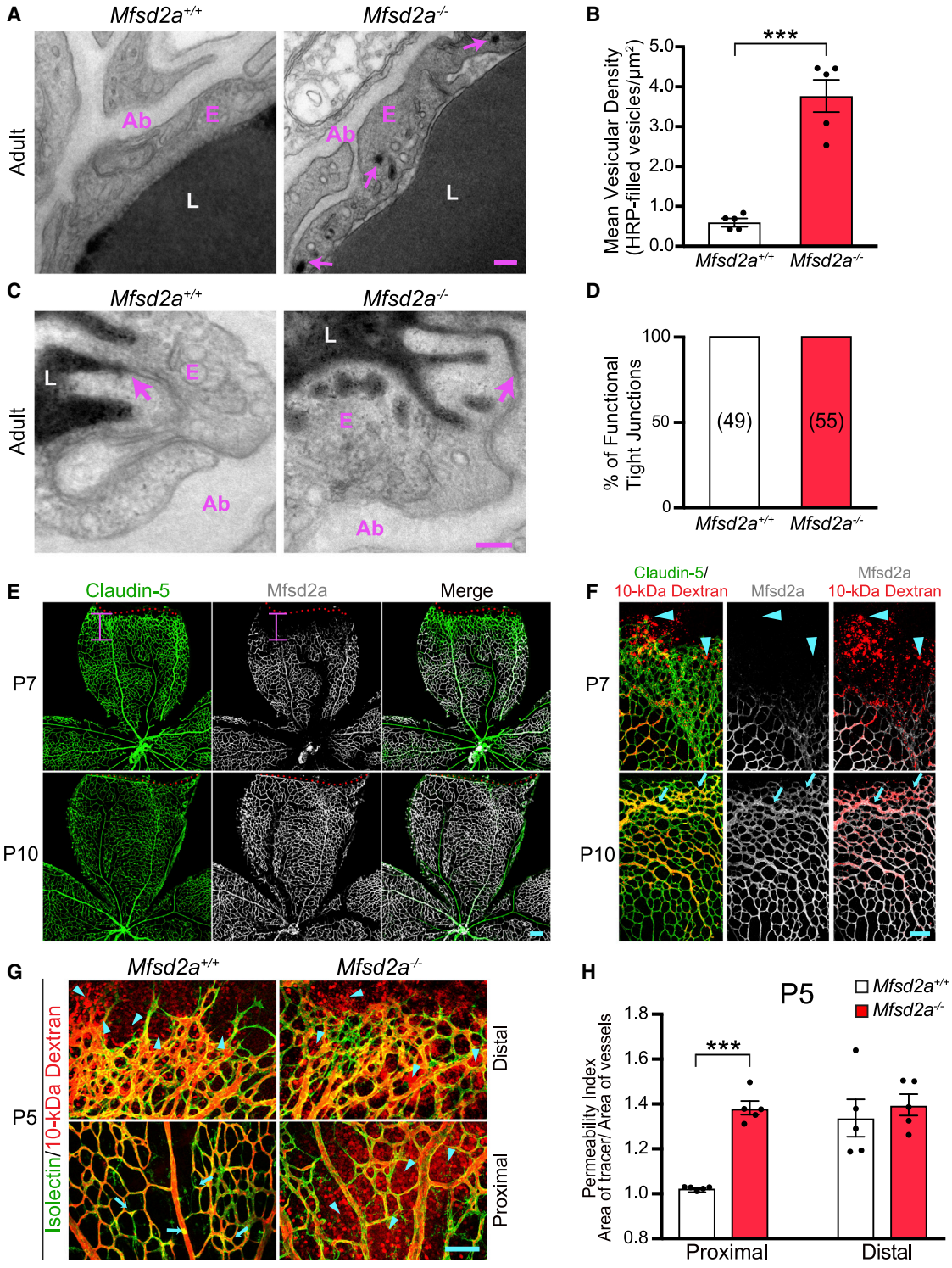

Figure 3. Elevated Levels of Transcytosis Deter Functional BRB Formation

(A) Transcytosis is increased in *Mfsd2a*$^{-/-}$ mice. Many tracer-filled vesicles (arrows) were observed in adult retinal endothelial cells from *Mfsd2a*$^{-/-}$, but not *Mfsd2a*$^{+/+}$, mice.

(B) Quantification of HRP-filled vesicles in retinal endothelial cells from adult *Mfsd2a*$^{+/+}$ and *Mfsd2a*$^{-/-}$ mice. Data are shown as mean ± SEM (n = 5 mice per genotype; each circle represents the average vesicular density from 18–20 vessels per mouse). Statistical significance was determined by unpaired t test.

(C) EM of the adult retina confirms that specialized tight junctions halt tracer product in both *Mfsd2a*$^{+/+}$ and *Mfsd2a*$^{-/-}$ adult mice.

(legend continued on next page)

from dextran tracer-injected pups. At P7, Mfsd2a protein is only present in proximal, impermeable vessels but absent in distal, leaky vessels (Figures 3E and 3F). In contrast, Claudin-5 is fully present at the distal vessels (Figures 3E and 3F). Importantly, Mfsd2a is absent from leaky, distal vessels during development (Figure 3F), and only by P10, when tracer is completely confined in the vessels, is Mfsd2a expression present at the distal vessels (Figures 3E and 3F). Thus, the spatio-temporal expression of Mfsd2a correlates with the gradual suppression of transcytosis and the development of a functional BRB.

Elevated Levels of Transcytosis Deter Functional BRB Formation

If the timing of the gradual suppression of transcytosis governs the development of a functional BRB, then altered regulation of transcytosis should affect functional BRB development. To test this idea, we examined the time course of functional BRB formation in two mutant mice with either increased or decreased transcytosis. First, we injected 10-kDa dextran tracers into *Mfsd2a*$^{-/-}$ mice and wild-type littermates at P5, P10, and adult ages. In P5 *Mfsd2a*$^{+/+}$ wild-type mice, tracer leaked from distal vessels but was confined in proximal vessels (Figures 3G and 3H). However, in P5 *Mfsd2a*$^{-/-}$ mice, tracer leaked from both distal and proximal vessels (Figures 3G and 3H), similar to what we observed in P1 wild-type pups (Figure 1C). Even at P10 and adulthood, this leaky phenotype persisted, indicating that failure to suppress transcytosis results in incomplete formation of a functional BRB (Figure S4).

Precocious Suppression of Transcytosis Accelerates Functional BRB Formation

We next tested whether precocious suppression of transcytosis during development accelerates functional BRB formation. Among various transcytotic pathways, peripheral endothelial cells frequently utilize the caveolae-pathway (Tuma and Hubbard, 2003). *Caveolin-1* (*Cav-1*) knockout mice lack caveolae vesicles throughout the endothelium (Drab et al., 2001; Razani et al., 2001) but display normal tight junctions in CNS barriers (Knowland et al., 2014). EM analysis of distal retinal vessels from P8 and P10 *Cav-1*$^{+/+}$ wild-type retinas revealed decreased vesicular density from P8 to P10 (Figures 4A and 4B). However, in *Cav-1*$^{-/-}$ mice, vesicular density was already low at P8 (Figures 4A and 4B), indicating a precocious suppression of transcytosis in the BRB. To examine the impact of precocious suppression of transcytosis on functional BRB formation, we intravenously injected bovine serum albumin (BSA), known to be transported via caveolae vesicles in lung endothelial cells (Schubert et al., 2001), in *Cav-1*$^{+/+}$ and *Cav-1*$^{-/-}$ mice at P8. In *Cav-1*$^{+/+}$ wild-type littermate mice, we observed BSA leakage into the retinal parenchyma from distal vessels (Figures 4C and 4D). However, in *Cav-1*$^{-/-}$ mice, BSA was confined throughout the vasculature, indicating that a functional BRB had formed at P8 instead of P10 (Figures 4C and 4D). This time shift in BRB impermeability demonstrates that precocious suppression of transcytosis results in an earlier formation of a functional BRB.

DISCUSSION

This study provides the first spatio-temporal characterization of functional BRB formation and establishes the BRB as a tractable model system for future study of CNS barriers. Using this system, we unexpectedly found that suppression of transcytosis is a principal contributor in the normal development of a functional barrier. We demonstrated that during BRB development, budding CNS endothelial cells already display functional tight junctions as early as vessel ingression but have not yet suppressed transcytosis. Thus, the leakiness of the developing retinal vasculature is entirely due to transcytosis. A functional BRB is established days later, only after transcytosis is gradually suppressed in BRB endothelial cells (Figure S5). In contrast to the prevailing notion in the field emphasizing the role of tight junctions in barrier function, our findings support an emerging view that transcytosis also plays a key role in regulating CNS barrier permeability and indicate that while specialized tight junctions are intrinsic to retinal endothelial cells, suppression of transcytosis is induced by CNS environmental cues during development. Our findings revealed that CNS endothelial cells have a developmental program that actively inhibits transcytosis to ensure barrier function. Finally, unregulated BRB dysfunction is a pathological feature of many ocular diseases (Klaassen et al., 2013). Our findings may offer insights to improving CNS drug delivery as manipulating transcytosis can transport different size cargos, including compounds less than 1 kDa to large macromolecules. Furthermore, genes that regulate transcytosis can be targeted to repair CNS barriers to treat neurodegenerative diseases.

(D) Quantification of functional tight junctions from *Mfsd2a*$^{+/+}$ and *Mfsd2a*$^{-/-}$ adult mice (n = 5 mice per genotype; 18–20 vessels analyzed per mouse; number of tight junctions analyzed are displayed in parentheses).

(E) Immunostaining for Claudin-5 (green) and Mfsd2a (white) on P7 and P10 retinas shows the lack of Mfsd2a expression in nascent, distal vessels at P7. The red dash lines indicate the angiogenic front as determined by Claudin-5 expression, and the pink bar indicates the length from the angiogenic front to the appearance of Mfsd2a expression. In contrast to P7, Mfsd2a is expressed in the distal vessels at P10 (n = 5 mice per age).

(F) Mfsd2a expression correlates with functional BRB formation. Immunostaining for Claudin-5 and Mfsd2a in retinas from 10-kDa dextran-injected P7 and P10 mice shows that, at P7, extravasation of tracer (arrowheads) occurs at nascent vessels where Mfsd2a is absent. At P10, tracer is confined (arrows) in distal vessels where Mfsd2a is expressed (n = 5 mice per age).

(G) Genetic ablation of *Mfsd2a* results in incomplete formation of the functional BRB. After intravenous injection of 10-kDa dextran in P5 *Mfsd2a*$^{+/+}$ and *Mfsd2a*$^{-/-}$ pups, tracer was confined (arrow) in proximal vessels (bottom) but leaked from distal vessels (top) in *Mfsd2a*$^{+/+}$ mice (arrowheads). In contrast, tracer leaked into the retinal parenchyma from both proximal and distal vessels in *Mfsd2a*$^{-/-}$ mice (arrowheads).

(H) Permeability index from proximal and distal regions of P5 *Mfsd2a*$^{-/-}$ and *Mfsd2a*$^{+/+}$ littermates. Data are shown as mean ± SEM (n = 5 mice per genotype; each circle represents the average permeability from each mouse). Statistical significance was determined by unpaired t test. ***$p < 0.001$. Scale bars represent 100 nm in (A) and (C) and 100 μm in (E), (F), and (G).

See also Figure S4.

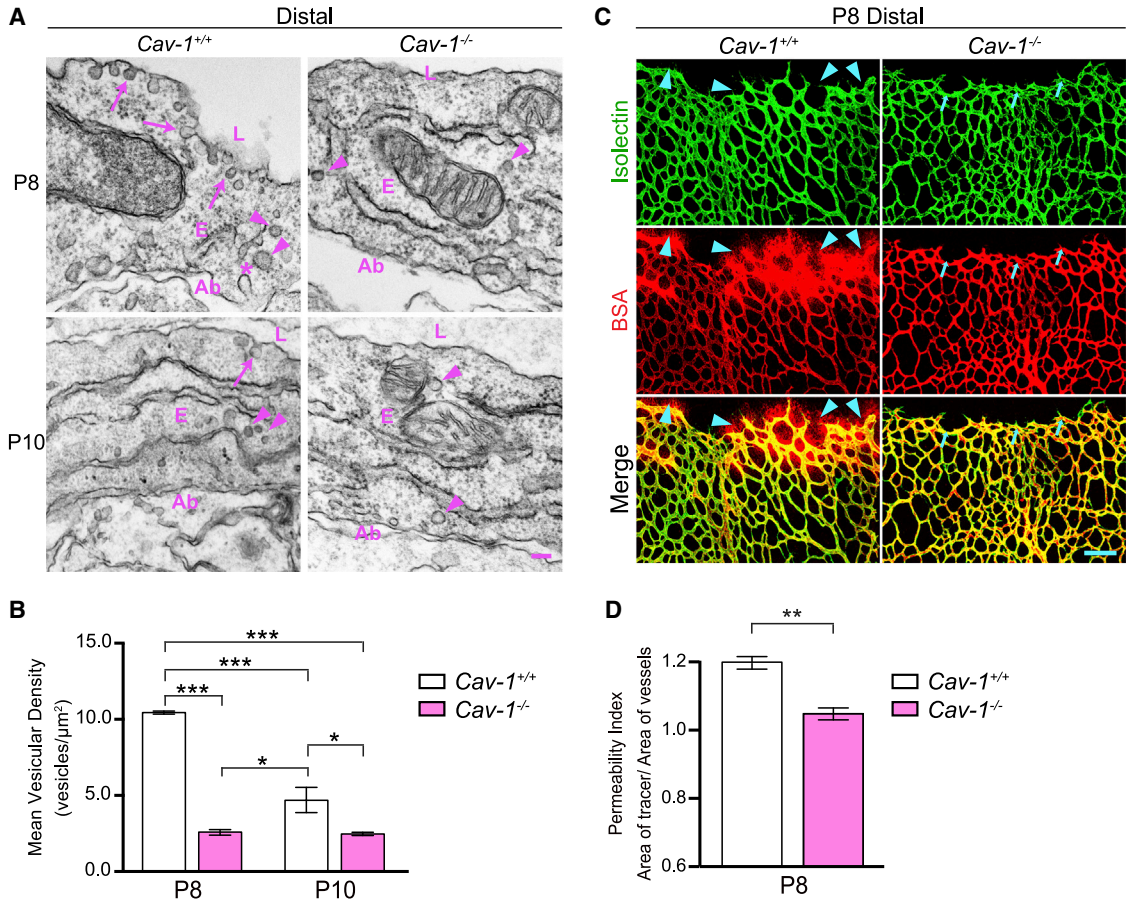

Figure 4. Precocious Suppression of Transcytosis Accelerates Functional BRB Formation

(A) Precocious suppression of transcytosis is observed in *Cav-1*$^{-/-}$ retinas. EM in distal vessels at P8 (top) reveals many vesicles associated with luminal (arrows) and abluminal (*) membranes and in the cytoplasm (arrowheads) in *Cav-1*$^{+/+}$ endothelial cells. *Cav-1*$^{-/-}$ endothelial cells have drastically reduced numbers of vesicles. At P10 (bottom), few vesicles are observed in both *Cav-1*$^{+/+}$ and *Cav-1*$^{-/-}$ distal vessels.

(B) Quantifications of vesicles in distal vessels from *Cav-1*$^{+/+}$ and *Cav-1*$^{-/-}$ mice at P8 and P10. Data are presented as mean ± SEM (n = 3 mice per age per genotype, 15–20 vessels analyzed per mouse). Statistical significance was determined by two-way ANOVA with a post hoc Bonferroni multiple comparison adjustment.

(C) Intravenous injection of BSA (red) in P8 pups reveals tracer leakage in the retinal parenchyma from distal vessels of *Cav-1*$^{+/+}$ (arrowheads), but not *Cav-1*$^{-/-}$, mice.

(D) Permeability index from distal regions of P8 *Cav-1*$^{+/+}$ and *Cav-1*$^{-/-}$ littermates. Data are presented as mean ± SEM (n = 3–4 mice per genotype). Statistical significance was determined by unpaired t test. *$p < 0.05$; **$p < 0.01$; ***$p < 0.001$. L, lumen; E, endothelial cells; Ab, abluminal. Scale bars represent 100 nm in (A) and 100 μm in (C).

What are the molecular mechanisms that induce CNS endothelial cells to gradually suppress transcytosis to develop a functional BRB? Pericytes ensheathing CNS endothelial cells are the most promising candidates, as pericyte-deficient mice have leaky barriers in brain and retina, aberrant tight junctions, elevated transcytosis, and reduced Mfsd2a protein at the blood-brain barrier (Armulik et al., 2010; Bell et al., 2010; Ben-Zvi et al., 2014; Daneman et al., 2010; Keskin et al., 2015; Sweeney et al., 2016; Winkler et al., 2011). Using NG2:DsRed reporter mice, which have labeled retinal mural cells, we examined pericyte coverage and density during BRB development and found that pericytes ensheath blood vessels at P1 (Figure S2A). In P5 retinas, we find about a 1:1 pericyte-to-endothelial-cell ratio throughout the retina (Figures S2B–S2D), including distal, nascent, leaky vessels, where Mfsd2a protein is absent (Figure S2E). This suggests that the differentiation state of pericytes or inductive factors derived from pericytes during development are likely the key mechanisms that induce CNS endothelial cells to suppress transcytosis for functional BRB formation. Indeed, the loss of function of two transcription factors, *foxc1* and *foxf2*, in CNS pericytes actually increases CNS pericyte density but still results in blood-brain barrier breakdown (Reyahi et al., 2015; Siegenthaler et al., 2013), suggesting that pericyte differentiation state, but not necessarily pericyte coverage or density per se, is important for blood-brain barrier integrity. Therefore, it is critical for future work to identify the pericyte-derived factors that mediate the gradual suppression of transcytosis for a functional BRB.

Canonical Wnt signaling is the best characterized signal for CNS angiogenesis and barrier formation (Daneman et al., 2009; Liebner et al., 2008; Stenman et al., 2008). In the retina, loss of function of the ligand (Norrin), receptor (Frizzled-4), co-receptors (Lrp5 and Tspan12), and downstream transcription factor (β-catenin) all result in impaired retinal angiogenesis and BRB breakdown (Junge et al., 2009; Wang et al., 2012; Ye et al., 2009; Zhou et al., 2014). Moreover, emerging evidence suggests that canonical Wnt signaling regulates tight junction function in CNS barriers, as loss of function of canonical Wnt signaling decreases Claudin-5 and increases PLVAP protein expression, resulting in opened junctions at the blood-brain barrier (Tran et al., 2016; Wang et al., 2012; Zhou et al., 2014). Whether canonical Wnt signaling also regulates the gradual suppression of transcytosis is not clear. On one hand, recent studies demonstrated canonical Wnt signaling is essential in the tip cells of nascent sprouts (Ulrich et al., 2016; Vanhollebeke et al., 2015); yet, these nascent, distal vessels display bulk transcytosis and lack Mfsd2a during BRB development. But on the other hand, microarray analysis on retinas from canonical Wnt signaling-deficient mice showed that Mfsd2a is downregulated (Chen et al., 2012). Therefore, while canonical Wnt signaling regulates functional tight junctions in BRB endothelial cells, it is imperative that future studies elucidate whether canonical Wnt signaling also regulates the suppression of transcytosis.

It is intriguing that functional BRB formation and the shift in a homeostatic retinal microenvironment occurs by P10, a few days before mouse eyes open (Feller, 2009). Furthermore, it is notable that the timing of retinal barrier formation correlates with the development of the neural retina, particularly with retinal waves. Retinal waves are spontaneous neural activity in retinal ganglion cells during development and are thought to refine visual circuitry prior to eye opening and the onset of sensory-evoked neural activity (Huberman et al., 2008). It will be interesting to investigate whether the temporal correlation of BRB development and retinal waves implies cross-talk between functional BRB formation and neural function. While the acquisition of barrier properties is dependent on inductive cues from the neural environment, it is unclear whether neural activity, especially spontaneous activity during development, is involved in transmitting these inductive cues for BRB formation. Alternatively, the maturation of the BRB could influence the spatio-temporal formation of the retinal waves. Addressing whether there is causal relationship between BRB formation and retinal waves could shift thought paradigms in both vascular biology and neurobiology.

STAR★METHODS

Detailed methods are provided in the online version of this paper and include the following:

- KEY RESOURCES TABLE
- CONTACT FOR REAGENT AND RESOURCE SHARING
- EXPERIMENTAL MODEL AND SUBJECT DETAILS
- METHOD DETAILS
  - BRB Permeability Assay and Flatmount Retina Immunohistochemistry
  - Transmission Electron Microscopy
  - Light Microscopy
- QUANTIFICATION AND STATISTICAL ANALYSIS
  - Permeability Index Quantifications
  - Mean Vesicular Density and Functional Tight Junction Quantification
  - Pericyte Density and Coverage Quantifications
  - Statistical Analyses
- DATA AND SOFTWARE AVAILABILITY

SUPPLEMENTAL INFORMATION

Supplemental Information includes five figures and one data file and can be found with this article online at http://dx.doi.org/10.1016/j.neuron.2017.02.043.

AUTHORS CONTRIBUTIONS

B.W.C. and C.G. conceived and designed the project. B.W.C. performed experiments and data analysis. B.W.C. and C.G. wrote the manuscript.

ACKNOWLEDGMENTS

We thank E. Raviola for advice and discussion; J. Cohen, P. D'Amore, D. Ginty, L. Goodrich, B. Lacoste, and members of the Gu laboratory for comments on the manuscript; and HMS Electron Microscopy Core Facility and the Neurobiology Imaging Facility for consultation and instrumentation that supported this work (this facility is supported in part by the Neural Imaging Center as part of NINDS P30 Core Center grant NS072030). This research was supported by NIH Training Grant 5T32MH20017-15 (B.W.C.), Fritz Hoffmann-La Roche Research Grant #A16726-A23485 (C.G.), Fidelity Biosciences Research Initiative (C.G.), and NIH DP1 NS092473 Pioneer Award (C.G.). The research of C.G. was also supported in part by a Faculty Scholar grant from the Howard Hughes Medical Institute.

Received: August 2, 2016
Revised: November 14, 2016
Accepted: February 22, 2017
Published: March 22, 2017

REFERENCES

Andreone, B.J., Lacoste, B., and Gu, C. (2015). Neuronal and vascular interactions. Annu. Rev. Neurosci. *38*, 25–46.

Armulik, A., Genové, G., Mäe, M., Nisancioglu, M.H., Wallgard, E., Niaudet, C., He, L., Norlin, J., Lindblom, P., Strittmatter, K., et al. (2010). Pericytes regulate the blood-brain barrier. Nature *468*, 557–561.

Banks, W.A. (2016). From blood-brain barrier to blood-brain interface: new opportunities for CNS drug delivery. Nat. Rev. Drug Discov. *15*, 275–292.

Bell, R.D., Winkler, E.A., Sagare, A.P., Singh, I., LaRue, B., Deane, R., and Zlokovic, B.V. (2010). Pericytes control key neurovascular functions and neuronal phenotype in the adult brain and during brain aging. Neuron *68*, 409–427.

Ben-Zvi, A., Lacoste, B., Kur, E., Andreone, B.J., Mayshar, Y., Yan, H., and Gu, C. (2014). Mfsd2a is critical for the formation and function of the blood-brain barrier. Nature *509*, 507–511.

Blanchette, M., and Daneman, R. (2015). Formation and maintenance of the BBB. Mech. Dev. *138*, 8–16.

Chen, J., Stahl, A., Krah, N.M., Seaward, M.R., Joyal, J.-S., Juan, A.M., Hatton, C.J., Aderman, C.M., Dennison, R.J., Willett, K.L., et al. (2012). Retinal expression of Wnt-pathway mediated genes in low-density lipoprotein receptor-related protein 5 (Lrp5) knockout mice. PLoS ONE *7*, e30203.

Chow, B.W., and Gu, C. (2015). The molecular constituents of the blood-brain barrier. Trends Neurosci. *38*, 598–608.

Daneman, R., Agalliu, D., Zhou, L., Kuhnert, F., Kuo, C.J., and Barres, B.A. (2009). Wnt/beta-catenin signaling is required for CNS, but not non-CNS, angiogenesis. Proc. Natl. Acad. Sci. U.S.A. *106*, 641–646.

Daneman, R., Zhou, L., Kebede, A.A., and Barres, B.A. (2010). Pericytes are required for blood-brain barrier integrity during embryogenesis. Nature *468*, 562–566.

Drab, M., Verkade, P., Elger, M., Kasper, M., Lohn, M., Lauterbach, B., Menne, J., Lindschau, C., Mende, F., Luft, F.C., et al. (2001). Loss of caveolae, vascular dysfunction, and pulmonary defects in caveolin-1 gene-disrupted mice. Science *293*, 2449–2452.

Engelhardt, B., and Coisne, C. (2011). Fluids and barriers of the CNS establish immune privilege by confining immune surveillance to a two-walled castle moat surrounding the CNS castle. Fluids Barriers CNS *8*, 4.

Feller, M.B. (2009). Retinal waves are likely to instruct the formation of eye-specific retinogeniculate projections. Neural Dev. *4*, 24.

Fruttiger, M. (2007). Development of the retinal vasculature. Angiogenesis *10*, 77–88.

Hagan, N., and Ben-Zvi, A. (2015). The molecular, cellular, and morphological components of blood-brain barrier development during embryogenesis. Semin. Cell Dev. Biol. *38*, 7–15.

Huberman, A.D., Feller, M.B., and Chapman, B. (2008). Mechanisms underlying development of visual maps and receptive fields. Annu. Rev. Neurosci. *31*, 479–509.

Junge, H.J., Yang, S., Burton, J.B., Paes, K., Shu, X., French, D.M., Costa, M., Rice, D.S., and Ye, W. (2009). TSPAN12 regulates retinal vascular development by promoting Norrin- but not Wnt-induced FZD4/beta-catenin signaling. Cell *139*, 299–311.

Karnovsky, M.J. (1967). The ultrastructural basis of capillary permeability studied with peroxidase as a tracer. J. Cell Biol. *35*, 213–236.

Keskin, D., Kim, J., Cooke, V.G., Wu, C.-C., Sugimoto, H., Gu, C., De Palma, M., Kalluri, R., and LeBleu, V.S. (2015). Targeting vascular pericytes in hypoxic tumors increases lung metastasis via angiopoietin-2. Cell Rep. *10*, 1066–1081.

Klaassen, I., Van Noorden, C.J.F., and Schlingemann, R.O. (2013). Molecular basis of the inner blood-retinal barrier and its breakdown in diabetic macular edema and other pathological conditions. Prog. Retin. Eye Res. *34*, 19–48.

Knowland, D., Arac, A., Sekiguchi, K.J., Hsu, M., Lutz, S.E., Perrino, J., Steinberg, G.K., Barres, B.A., Nimmerjahn, A., and Agalliu, D. (2014). Stepwise recruitment of transcellular and paracellular pathways underlies blood-brain barrier breakdown in stroke. Neuron *82*, 603–617.

Liebner, S., Corada, M., Bangsow, T., Babbage, J., Taddei, A., Czupalla, C.J., Reis, M., Felici, A., Wolburg, H., Fruttiger, M., et al. (2008). Wnt/beta-catenin signaling controls development of the blood-brain barrier. J. Cell Biol. *183*, 409–417.

Obermeier, B., Daneman, R., and Ransohoff, R.M. (2013). Development, maintenance and disruption of the blood-brain barrier. Nat. Med. *19*, 1584–1596.

Raviola, G. (1977). The structural basis of the blood-ocular barriers. Exp. Eye Res. *25* (*Suppl*), 27–63.

Razani, B., Engelman, J.A., Wang, X.B., Schubert, W., Zhang, X.L., Marks, C.B., Macaluso, F., Russell, R.G., Li, M., Pestell, R.G., et al. (2001). Caveolin-1 null mice are viable but show evidence of hyperproliferative and vascular abnormalities. J. Biol. Chem. *276*, 38121–38138.

Reese, T.S., and Karnovsky, M.J. (1967). Fine structural localization of a blood-brain barrier to exogenous peroxidase. J. Cell Biol. *34*, 207–217.

Reyahi, A., Nik, A.M., Ghiami, M., Gritli-Linde, A., Pontén, F., Johansson, B.R., and Carlsson, P. (2015). Foxf2 is required for brain pericyte differentiation and development and maintenance of the blood-brain barrier. Dev. Cell *34*, 19–32.

Schneeberger-Keeley, E.E., and Karnovsky, M.J. (1968). The ultrastructural basis of alveolar-capillary membrane permeability to peroxidase used as a tracer. J. Cell Biol. *37*, 781–793.

Schubert, W., Frank, P.G., Razani, B., Park, D.S., Chow, C.W., and Lisanti, M.P. (2001). Caveolae-deficient endothelial cells show defects in the uptake and transport of albumin in vivo. J. Biol. Chem. *276*, 48619–48622.

Siegenthaler, J.A., Choe, Y., Patterson, K.P., Hsieh, I., Li, D., Jaminet, S.-C., Daneman, R., Kume, T., Huang, E.J., and Pleasure, S.J. (2013). Foxc1 is required by pericytes during fetal brain angiogenesis. Biol. Open *2*, 647–659.

Stahl, A., Connor, K.M., Sapieha, P., Chen, J., Dennison, R.J., Krah, N.M., Seaward, M.R., Willett, K.L., Aderman, C.M., Guerin, K.I., et al. (2010). The mouse retina as an angiogenesis model. Invest. Ophthalmol. Vis. Sci. *51*, 2813–2826.

Stenman, J.M., Rajagopal, J., Carroll, T.J., Ishibashi, M., McMahon, J., and McMahon, A.P. (2008). Canonical Wnt signaling regulates organ-specific assembly and differentiation of CNS vasculature. Science *322*, 1247–1250.

Stewart, P.A., and Wiley, M.J. (1981). Developing nervous tissue induces formation of blood-brain barrier characteristics in invading endothelial cells: a study using quail–chick transplantation chimeras. Dev. Biol. *84*, 183–192.

Stone, J., Itin, A., Alon, T., Pe'er, J., Gnessin, H., Chan-Ling, T., and Keshet, E. (1995). Development of retinal vasculature is mediated by hypoxia-induced vascular endothelial growth factor (VEGF) expression by neuroglia. J. Neurosci. *15*, 4738–4747.

Sweeney, M.D., Ayyadurai, S., and Zlokovic, B.V. (2016). Pericytes of the neurovascular unit: key functions and signaling pathways. Nat. Neurosci. *19*, 771–783.

Tran, K.A., Zhang, X., Predescu, D., Huang, X., Machado, R.F., Göthert, J.R., Malik, A.B., Valyi-Nagy, T., and Zhao, Y.-Y. (2016). Endothelial β-catenin signaling is required for maintaining adult blood-brain barrier integrity and central nervous system homeostasis. Circulation *133*, 177–186.

Tuma, P., and Hubbard, A.L. (2003). Transcytosis: crossing cellular barriers. Physiol. Rev. *83*, 871–932.

Ulrich, F., Carretero-Ortega, J., Menéndez, J., Narvaez, C., Sun, B., Lancaster, E., Pershad, V., Trzaska, S., Véliz, E., Kamei, M., et al. (2016). Reck enables cerebrovascular development by promoting canonical Wnt signaling. Development *143*, 147–159.

Vanhollebeke, B., Stone, O.A., Bostaille, N., Cho, C., Zhou, Y., Maquet, E., Gauquier, A., Cabochette, P., Fukuhara, S., Mochizuki, N., et al. (2015). Tip cell-specific requirement for an atypical Gpr124- and Reck-dependent Wnt/β-catenin pathway during brain angiogenesis. eLife *4*, 4.

Wang, Y., Rattner, A., Zhou, Y., Williams, J., Smallwood, P.M., and Nathans, J. (2012). Norrin/Frizzled4 signaling in retinal vascular development and blood brain barrier plasticity. Cell *151*, 1332–1344.

Winkler, E.A., Bell, R.D., and Zlokovic, B.V. (2011). Central nervous system pericytes in health and disease. Nat. Neurosci. *14*, 1398–1405.

Winkler, E.A., Sengillo, J.D., Sagare, A.P., Zhao, Z., Ma, Q., Zuniga, E., Wang, Y., Zhong, Z., Sullivan, J.S., Griffin, J.H., et al. (2014). Blood-spinal cord barrier disruption contributes to early motor-neuron degeneration in ALS-model mice. Proc. Natl. Acad. Sci. USA *111*, E1035–E1042.

Ye, X., Wang, Y., Cahill, H., Yu, M., Badea, T.C., Smallwood, P.M., Peachey, N.S., and Nathans, J. (2009). Norrin, frizzled-4, and Lrp5 signaling in endothelial cells controls a genetic program for retinal vascularization. Cell *139*, 285–298.

Zhao, Z., Nelson, A.R., Betsholtz, C., and Zlokovic, B.V. (2015). Establishment and dysfunction of the blood-brain barrier. Cell *163*, 1064–1078.

Zhou, Y., Wang, Y., Tischfield, M., Williams, J., Smallwood, P.M., Rattner, A., Taketo, M.M., and Nathans, J. (2014). Canonical WNT signaling components in vascular development and barrier formation. J. Clin. Invest. *124*, 3825–3846.

Zlokovic, B.V. (2008). The blood-brain barrier in health and chronic neurodegenerative disorders. Neuron *57*, 178–201.

STAR★METHODS

KEY RESOURCES TABLE

REAGENT or RESOURCE	SOURCE	IDENTIFIER
Antibodies		
Rabbit monoclonal α-ERG1/2/3	Abcam	Cat# ab92513, RRID: AB_2630401
Rabbit polyclonal α-Mfsd2a	Cell Signaling Technology	Still under development, Cat# 14-87 Mfsd2a, RRID: AB_2617168
Mouse monoclonal α-Claudin-5	Thermo Fisher Scientific	Cat# 352588 Lot# RRID: AB_2532189
Chemicals, Peptides, and Recombinant Proteins		
Isolectin GS-IB4 From Griffonia simplicifolia	Thermo Fisher Scientific	Cat #I21411
Sulfo-NHS-Biotin	Thermo Fisher Scientific	Cat #21335
3-kDa Dextran conjugated to Tetramethylrhodamine	Thermo Fisher Scientific	Cat #D3308
10-kDa Dextran conjugated to Tetramethylrhodamine	Thermo Fisher Scientific	Cat #D1868
Bovine serum albumin conjugated to Alexa 555	Thermo Fisher Scientific	Cat #A34786
Horseradish peroxidase type II	Sigma-Aldrich	P8250-50KU
Experimental Models: Organisms/Strains		
Wild-type Swiss-Webster mice	Charles River	Strain 024
B6;129S5-Mfsd2atm1Lex/Mmucd	Mouse Biology Program, University of California, Davis	MMRRC strain 032467-UCD; RRID: MGI:5755244
B6.Cg-Cav1tm1Mls/J	Jackson Laboratory	JAX; 007083, MGI Cat# 4418046, RRID: MGI:4418046
Tg(Cspg4-DsRed.T1)1Akik/J (*NG2:DsRed*)	Jackson Laboratory	JAX; 008241, RRID: MGI:3796133
Oligonucleotides		
Primers: Mfsd2a DNA 314F-1 (WT): CCTGGTTTGCTAAGTGCTAGC DNA 314R-2 (WT): GTTCACTGGCTTGGAGGATGC KO 314F-5 (KO): CACTTCCTAAAGCCTTACTTC NEO3a (KO): GCAGCGCATCGCCTTCTATC	Integrated DNA Technologies	N/A
Primers: Cav1 Cav1 661 WT Fwd: GCA CAC CAA GGA GAT TGA CC Cav1 200 MuT Fwd: CTC CAG ACT GCC TTG GGA AAA Cav1 661: CTT GGC TGT CAC CAC ACA C	Integrated DNA Technologies	N/A
Primers: DsRed DsRed Fwd: TTC CTT CGC CTT ACA AGT CC DsRed Rev:GAG CCG TAC TGG AAC TGG	Integrated DNA Technologies	N/A
Software and Algorithms		
Prism Version 7	GraphPad	https://www.graphpad.com/scientific-software/prism/
ImageJ custom macro for quantification of permeability	This paper	Data S1

CONTACT FOR REAGENT AND RESOURCE SHARING

For further information and requests for reagents in this study, please contact Lead Contact Chenghua Gu (chenghua_gu@hms.harvard.edu).

EXPERIMENTAL MODEL AND SUBJECT DETAILS

Wild-type Swiss-Webster mice (Charles River Laboratory; Strain 024) were used for postnatal BRB functionality assays. Day of birth was defined as postnatal day zero (P0). Both males and females were used in this study. *Mfsd2a*$^{-/-}$ mice (Ben-Zvi et al., 2014) (MGI Cat# 5755244, RRID: MGI:5755244) were maintained on a C57Bl/129 background (currently backcrossed to C57Bl for the 5th generation) and used to determine incomplete BRB formation and for validation of the Mfsd2a antibody in retinas. *Cav-1*$^{-/-}$ mice

(maintained on congenic C57Bl background) (Razani et al., 2001) (JAX; 007083, MGI Cat# 4418046, RRID: MGI:4418046) were maintained in C57BL/6J and used to determine precocious BRB development. *NG2:DsRed* mice (JAX; 008241, RRID: MGI:3796133) (maintained on congenic C57Bl background) were used to determine pericyte density and coverage during functional BRB development. Littermates of either sex were randomly assigned to experimental groups. A maximum of five adult mice were maintained in one cage. For postnatal mice, the litter and two adult mice were maintained in one cage. Mice were maintained on a 12 light/12 dark cycle. All animals were treated according to institutional and US National Institutes of Health (NIH) guidelines approved by the Institutional Animal Care and Use Committee (IACUC) at Harvard Medical School.

METHOD DETAILS

BRB Permeability Assay and Flatmount Retina Immunohistochemistry

Neonatal pups and adults (8 −10 weeks old) were deeply anesthetized. Sulfo-NHS-Biotin (Thermo Fisher Scientific; 21335), 3-kDa or 10-kDa dextran conjugated to Tetramethylrhodamine (Thermo Fisher Scientific; D3308 and D1868, respectively), and bovine serum albumin conjugated to Alexa Fluor 555 (Thermo Fisher Scientific; A34786) were injected at 0.5 mg/g body weight for Sulfo-NHS-Biotin and 0.1 mg/g body weight for the rest of tracers as previously described (Armulik et al., 2010) into the left-ventricle with a 31 gauge, 0.3 cc insulin syringe. The heartbeat was monitored for a steady heartbeat that was continuous for 5 min. If the heartbeat stopped during the 5 min circulation, the animals were excluded due to poor circulation of the tracer. After 10 min of tracer circulation of the tracer, both eyes were enucleated. Eyes were fixed briefly (5-10 min) in 4% PFA. Retinas were dissected out in 4% PFA to ensure dye fixation within the tissue. Retinas were fixed overnight in 4% PFA at 4°C and washed in PBS three times for 5 min each the next day. Retinas were incubated in blocking buffer (10% normal goat serum, 3% bovine serum albumin, and 0.5% Triton X-100 in PBS) for 1 hr at room temperature. Isolectin GS-IB4 conjugated to Alexa Fluor 488 (Thermo Scientific; I21411) or the following primary antibodies: rabbit α-ERG1/2/3 (Abcam Cat# ab92513, RRID: AB_2630401, 1:200), rabbit α-Mfsd2a (Cell Signaling Technology still under development, Cat# 14-87 Mfsd2a, RRID: AB_2617168, 1:200) and mouse α-Claudin-5, (Thermo Fisher Scientific Cat# 352588 Lot# RRID: AB_2532189, 1:400) were then incubated in blocking buffer overnight at 4°C. Retinas were then washed in PBS three times for 5 min and incubated with the Alexa Fluor conjugated secondary antibodies (Thermo Fisher Scientific; 1:300) for 4 hr at room temperature. Retinas were washed in PBS three times for 10 min and flat-mounted with vitreal surface facing up using Prolong Gold (Molecular Probe, 1747013).

Transmission Electron Microscopy

EM imaging of adult and neonatal HRP injected retinas was carried out as described previously (Ben-Zvi et al., 2014). HRP (0.5 mg/g body weight Sigma Aldrich, HRP type II) was dissolved in 0.4 mL of PBS and injected into the retro-orbital sinus of deeply anaesthetized mice. After 15 or 30 min of HRP circulation for pups or adults, respectively, the contralateral eye of the sinus injection was enucleated. The eye was dissected immediately in 4% PFA and fixed by immersion in a 0.1 M sodium-cacodylate-buffered mixture (5% glutaraldehyde and 4% PFA) for 1 hr at room temperature followed by overnight fixation in 4% PFA at 4°C. Following fixation, the tissue was washed three times and then overnight in 0.1 M sodium-cacodylate buffer. Retinas were incubated for 25 or 45 min for neonatal or adults, respectively, at room temperature in 0.05 M Tris-HCl pH 7.6 buffer, containing 5.0 mg per 10 mL of 3-39 diaminobenzidine (DAB, Sigma Aldrich) with 0.01% hydrogen peroxide. After DAB staining, the retinal vasculature could be visualized. The distal edge of the vasculature and proximal edge of optic nerve head were micro-dissected and samples were lightly nicked to provide orientation to cut ultrathin sections. Samples were then postfixed in 1% osmium tetroxide and 1.5% potassium ferrocyanide, dehydrated, and embedded in epoxy resin. P8 and P10 *Cav-1*$^{-/-}$ and wild-type littermate retinas were processed as stated above without HRP injections and fixed for 5 days in 0.5% glutaraldehyde in 4% PFA prepared in 0.1 mM phosphate buffer, pH 7.4 and without DAB staining. Retinas were washed three times and then overnight in 0.1 M sodium-cacodylate buffer. Ultrathin sections (80 nm) were then cut from the block surface, collected on copper grids, stained with Reynold's lead citrate, and examined under a 1200EX electron microscope (JEOL) equipped with a 2k CCD digital camera (AMT). The nick could be visualized on the ultrathin section.

Light Microscopy

Olympus FluoView FV1000 and FV1200 laser scanning confocal microscopes (20x, 0.75 N.A. and 40x, 1.4 N.A.) and an Olympus VS 120 slide scanner (10x, 0.4 N.A.) were used for imaging flatmount retinas. Images were processed using Adobe Photoshop, Illustrator, Olympus Fluoview and FIJI (NIH).

QUANTIFICATION AND STATISTICAL ANALYSIS

Permeability Index Quantifications

All quantifications were performed blind with a self-written FIJI (NIH) macro (see Data S1). Six to eight 290 μm x 290 μm x 5 μm thick z stack images of the vessels of distal and proximal regions of the primary plexus, six to eight 317 um x 317 um of deeper plexus and intermediate plexus at 3-5 μm thick z stack images and six to eight 635 μm x 635 μm of *Mfsd2a*$^{-/-}$ and *Cav-1*$^{-/-}$ with their respective wild-type littermates per mouse retina were max Z-projected, filtered with a Gaussian blur and background subtracted via rolling ball

method. Distal vessel images were acquired by aligning the field of view to capture the retinal tip cells and proximal images were acquired by aligning the field view slightly after the optic nerve head. The isolectin and tracer signals were auto-thresholded by the same method for all ages and genotypes. The area of the segmented vessel and the tracer were determined. The ratio of the area of the tracer and the area of the vessel was then calculated. A ratio of 1 means that the tracer and vessel area is the same, indicating a functional barrier. The average of the ratios from the six to eight images is considered one biological sample.

Mean Vesicular Density and Functional Tight Junction Quantification

15-20 vessels from retinas were imaged under electron microscopy. To quantify mean vesicular density, tracer-filled vesicles were counted and divided by the area of the cytoplasm of the endothelial cells (excluding the nucleus). To determine percentage of functional tight junctions, the number of tight junctions that halt the tracer at the luminal side without parenchymal leakage was counted and divided by the total number of tight junctions counted.

Pericyte Density and Coverage Quantifications

Retinas from P5 NG2:DsRed mice were stained for ERG1/2/3 (endothelial nuclei marker) and isolectin. Images of four retinal leafs per retina were acquired. Images were max Z-projected, filtered with a Gaussian blur and background subtracted via rolling ball method. To quantify pericyte density, the NG2:DsRed signal was also applied with a minimum filter to reduce weak signal in the processes of pericytes but retain high signals in the soma. 250 μm x 250 μm field of views were analyzed from 0 μm (slightly before the optic nerve head) to the distal vessels (up to 1750 μm). Images were then segmented for NG2:DsRed and ERG1/2/3 signals and particles were then counted to determine pericyte density (NG2:DsRed+/ERG+ particles). To quantify pericyte coverage which is displayed as NG2:DsRed area/Isolectin area, a minimum filter was not applied but instead, images were simply segmented for NG2:DsRed signal and Isolectin signal.

Statistical Analyses

Quantitative data are expressed as the mean ± s.e.m. The sample size, what each ''n'' represents, the statistical tests used and the result of the statistical test are indicated in each respective Figure Legend. No statistical methods were used to predetermine sample sizes, but our sample sizes are comparable to those reported in previous publications (Armulik et al., 2010; Ben-Zvi et al., 2014). Statistical analyses were performed using Prism 6 (GraphPad). Differences between two different groups (either age or genotype) were analyzed by unpaired t test. Differences among different age groups were analyzed by one-way ANOVA followed by a Bonferroni's multiple comparisons correction. Differences among different age groups and genotype were analyzed by two-way ANOVA followed by a Bonferroni's multiple comparisons correction. Normality and equality of variances among the groups were analyzed by Brown-Forsythe tests. P values less than 0.05 were considered significant.

DATA AND SOFTWARE AVAILABILITY

ImageJ macro for quantification of images to determine the permeability index is provided as Data S1.